



Available online at www.sciencedirect.com

ScienceDirect

Geochimica et Cosmochimica Acta 238 (2018) 85–101

**Geochimica et
Cosmochimica
Acta**

www.elsevier.com/locate/gca

Zinc isotopic systematics of Kamchatka-Aleutian arc magmas controlled by mantle melting

Jian Huang ^{a,*}, Xing-Chao Zhang ^a, Sha Chen ^a, Limen Tang ^b, Gerhard Wörner ^c,
Huimin Yu ^a, Fang Huang ^{a,*}

^a CAS Key Laboratory of Crust-Mantle Materials and Environments, School of Earth and Space Sciences, University of Science and Technology of China, Hefei 230026, China

^b Second Institute of Oceanography, SOA, China

^c Division of Geochemistry, Geosciences Center, Georg-August-Universität Göttingen, 37077 Göttingen, Germany

Received 22 February 2018; accepted in revised form 3 July 2018; Available online 11 July 2018

Abstract

Geochemical characteristics of arc magmas reflect incorporation of subducted materials to their mantle wedge sources in subduction zones. Subduction component addition has been proposed to modify the Zn isotopic budget of arc magmas. However, the lack of a systematic study on Zn isotopic compositions of arc magmas hampers a better understanding of Zn isotope behavior in subduction zones. To address this issue, we have determined Zn isotopic compositions of 37 well-characterized arc rocks from the Kamchatka and Central-Eastern Aleutian arcs. These rocks record contributions of fluids and melts derived from altered oceanic crust (AOC) without overprints of sediment melts and thus allow focus on the potential effects of AOC-derived fluids and melts on the Zn isotopic budget of arc magmas. For comparison, nine basalts from the Gakkel, Mid-Atlantic and Southeast Indian Ridges, and the Lau Basin and nine adakites from Central America were also analyzed. Rocks from the Kamchatka-Aleutian arcs have $\delta^{66}\text{Zn}$ from 0.16 to 0.31‰ that are mostly similar to those of mid-ocean ridge basalts (MORBs), back-arc basin basalts (BABBs), and adakites ($\delta^{66}\text{Zn} = 0.23\text{--}0.33\text{\textperthousand}$), but a significant number of arc samples also display $\delta^{66}\text{Zn}$ higher than that of the depleted MORB-type mantle (DMM), indicating Zn isotope fractionation during magmatic processes and/or modifications of the mantle wedge Zn isotopic budget by incorporation of AOC-derived fluids and melts.

The lack of correlations of $\delta^{66}\text{Zn}$ with geochemical indicators of magma differentiation (e.g., MgO, SiO₂, and Zn/Fe_T) indicate that fractionation of olivine, pyroxene, and magnetite has a limited effect on the Zn isotopic compositions of arc magmas. Even though the mantle sources of arc rocks investigated here are strongly affected by AOC-derived fluids and melts that have higher $\delta^{66}\text{Zn}$ compared to the DMM, we observe no systematic variations of $\delta^{66}\text{Zn}$ with indicators of subduction components (e.g., Ba/La, Ba/Th, Sr/Y, Hf/Lu and ⁸⁷Sr/⁸⁶Sr). This suggests that insignificant transport of Zn from the subducting Pacific slab to the Kamchatka and Central-Eastern Aleutian mantle wedge. Our model calculations suggest that the observed offset of $\delta^{66}\text{Zn}$ between the mantle and arc magmas can be attributed to isotope fractionation during partial melting with no need for contributions from subduction components.

© 2018 Elsevier Ltd. All rights reserved.

Keywords: Zn isotopes; Arc magmas; Subduction components; Partial melting; Magma differentiation

* Corresponding authors.

E-mail addresses: jianhuang@ustc.edu.cn (J. Huang), fhuang@ustc.edu.cn (F. Huang).

1. INTRODUCTION

Arc magmas at convergent plate margins display a number of distinct geochemical features relative to magmas erupted at mid-ocean ridges, including the enrichment of large ion lithophile elements (LILEs) and light rare earth elements (LREEs), and the depletion of high field strength elements (HFSEs) (e.g., Pearce and Peate, 1995). Mid-ocean ridge basalts form via decompression melting of the upwelling asthenosphere mantle at nominally dry conditions, while most arc magmas originate from flux-melting of the mantle wedge above the subducting slab under hydrous conditions. Melting is triggered by fluids and/or melts liberated by dehydration and/or partial melting of sediments, the underlying basaltic oceanic crust and even the ultramafic serpentinites during oceanic plate subduction (e.g., Kelemen et al., 2007). These fluids and melts deliver slab-derived (i.e., subduction) components to the mantle wedge and finally to arc magmas (e.g., McCulloch and Gamble, 1991; Elliott et al., 1997; Metrich and Wallace, 2008). Thus, the compositions of arc magmas are determined by addition of subduction components, partial melting of the sub-arc mantle wedge that is generally more depleted than the source of MORBs (e.g., Woodhead et al., 1993; Nebel et al., 2015), and shallow differentiation in crustal magma chambers.

Apart from typical trace element patterns, radiogenic and stable isotopic compositions also allow characterization and identification of arc magma source components. This includes metal stable isotopes for many elements (e.g., Li, Mg, Fe, Mo, and Cu) (e.g., Tang et al., 2014; Liu et al., 2015; Nebel et al., 2015; König et al., 2016; Sossi et al., 2016; Teng et al., 2016). Recently, a growing number of Zn isotopic data shows that the $\delta^{66}\text{Zn}$ values are 0.18–0.55‰ for altered oceanic crust (AOC), –0.05 to 1.34‰ for sedimentary materials (e.g., carbonate/silicate sediments and shales) (Maréchal et al., 2000; Pichat et al., 2003; Bentahila et al., 2008; Pons et al., 2011; Little et al., 2014, 2016; Huang et al., 2016), and –0.48 to 0.52‰ for serpentinites (Pons et al., 2011, 2016). In contrast to highly heterogeneous Zn isotopic compositions in these potential subduction components, the normal mantle (i.e., the mantle that is not affected by metasomatism) represented by non-metasomatic peridotites have a homogeneous Zn isotopic composition ($\delta^{66}\text{Zn} = 0.16 \pm 0.06\text{\textperthousand}$, 2SD, Sossi et al., 2018; $0.18 \pm 0.06\text{\textperthousand}$, 2SD, Wang et al., 2017). This suggests that Zn isotopes may be a new and useful tracer of the nature of subduction components in arc magmatism and their potential contribution via recycling processes to the source of plume-related magmatism in intraplate settings (Liu et al., 2016; Pons et al., 2016; Wang et al., 2017).

The elevated $\delta^{66}\text{Zn}$ (0.57–0.89‰) in fluid-derived secondary olivines from the Kohistan Paleo-Island-Arc mantle have been attributed to metasomatism by isotopically heavy slab-derived fluids (Pons et al., 2016). Although previous studies have proposed that such heavy slab-derived Zn isotopic signatures should be recorded in arc magmatism (Pons et al., 2016), a systematic analysis of Zn isotopes

in arc magmas has not yet been done for a better understanding of the behavior of Zn isotopes in subduction zones. To the best of our knowledge, there are only six scattered data for Zn isotopes on fresh andesites from three volcanoes at convergent plate margins. Five andesites from the La Soufrière volcano, Northern Lesser Antilles and the Merapi volcano in the central of Java, Indonesia have $\delta^{66}\text{Zn}$ of 0.21–0.25‰ (Toutain et al., 2008; Chen et al., 2014), falling within the range of MORBs and ocean island basalts (OIBs, $\delta^{66}\text{Zn} = 0.24\text{--}0.40\text{\textperthousand}$, Herzog et al., 2009; Chen et al., 2013; Wang et al., 2017), but marginally higher than that of the normal mantle ($0.16 \pm 0.06\text{\textperthousand}$, Sossi et al., 2018). One andesite from Taiwan Island at the collision boundary between the Philippine and the Asian Continental Plate displays a heavy $\delta^{66}\text{Zn}$ of 0.55‰, which was proposed to reflect either the particular characteristics of Zn isotopic compositions in Taiwan rocks or input of isotopically heavy AOC-derived melts to the mantle wedge (Bentahila et al., 2008).

Even if subduction components mainly play a role in lowering the solidus of but do not modify the Zn isotopic budget of the mantle wedge, partial melting and magma differentiation still may have an effect on the Zn isotopic compositions of arc magmas. Previous studies have shown that mantle melting results in an enrichment of heavy Zn isotopes (e.g., ^{66}Zn) in the partial melts relative to the residual peridotites (Doucet et al., 2016; Wang et al., 2017; Sossi et al., 2018). Fractional crystallization of olivine and/or Fe-Ti oxides is likely to further enhance the heavy Zn isotope enrichment in the evolved melts (Chen et al., 2013).

In order to simultaneously examine the effect of mantle melting and magma differentiation on the Zn isotopic budget of arc magmas and to test whether their Zn isotopic compositions are sensitive to the contributions of subduction components (e.g., fluids and melts), we present the first systematic Zn isotope investigation on a set of 37 well-characterized magmatic rocks from the Kamchatka and Central-Eastern (CE) Aleutian arcs, including basalts, basaltic andesites, andesites, dacites, and intrusive equivalents. The samples that we analyzed have diverse compositions, experienced significant differentiation and represent mantle wedge sources that had been modified by fluids (e.g., EVF, CKD, and SR in Kamchatka) and slab melts (e.g., NCKD in Kamchatka; Atka and Umnak in CE Aleutians) derived from the subducted AOC without overprints of sediment melts (Churikova et al., 2001; Münker et al., 2004; Cai et al., 2015). Therefore, these samples allow us to assess the effects of magmatic processes and the role of AOC-derived fluids and melts on the Zn isotopic budget of arc magmas. For comparison, measurements were also carried out for seven MORBs from the Gakkel, Mid-Atlantic and Southeast Indian Ridges and two BABBs from the Lau Basin, because the previously-published Zn isotopic data for MORBs are scarce (only 6 in Wang et al., 2017). In addition, we also analyzed nine adakites from the Central American Volcanic Arc, which result from slab melting (Abratis and Wörner, 2001; Wegner et al., 2011), to constrain the Zn isotopic characteristics of AOC-derived melts.

2. GEOLOGICAL BACKGROUNDS AND SAMPLE DESCRIPTIONS

2.1. The Kamchatka arc

The Kamchatka arc is located at the convergent boundary of the Pacific and Eurasian plates (Fig. 1). The Pacific plate, carrying the 65 Ma old Emperor Seamount chain, presently subducts below Kamchatka at the rate of ~9 cm/yr (Geist and Scholl, 1994). At ~57°N, the Kamchatka and Aleutian arcs intersect at an angle of ~90° (Yogodzinski et al., 2001).

Twenty-seven Quaternary calc-alkaline volcanic rocks from the Kamchatka arc were analyzed for Zn isotopes in this study. Their major and trace element contents and Sr-Nd-Pb-Hf-O isotopic compositions have been previously reported (Dorendorf et al., 2000; Churikova et al., 2001; Münker et al., 2004). Twenty-four samples come from the Eastern Volcanic Front (EVF), the Central Kamchatka Depression (CKD) and the Sredinny Ridge (SR) that define a complete traverse across the arc at 56°N (Fig. 1). Most samples are basalts and basaltic andesites with SiO_2 from 47.4 to 55.8 wt%, MgO from 3.6 to 9.1 wt%, FeO_{T} ($\text{T} = \text{Total}$) from 5.2 to 11.1 wt%, and Zn from 50 to 110 ppm (Fig. 2, Churikova et al., 2001). Major and trace elements indicate variable olivine and clinopyroxene fractionation with some rocks affected by magnetite fractionation (Fig. 2, Churikova et al., 2001). An andesite and a more differentiated dacite from the EVF are also included to evaluate the influence of differentiation on Zn isotopic systematics in these lavas. Trace element (Fig. 3a) and Sr-Nd-Pb-Hf-O isotope systematics suggest that rocks from the 56°N arc traverse originate from a heterogeneous

mantle wedge, chemically affected by adding variable amounts of fluids derived from the subducting Pacific oceanic crust and the subducted Emperor seamount chain (Dorendorf et al., 2000; Churikova et al., 2001; Münker et al., 2004). A significant contribution from subducted sediments can be excluded based on low $^{207}\text{Pb}/^{204}\text{Pb}$ (<15.528) and $^{87}\text{Sr}/^{86}\text{Sr}$ (<0.703665) ratios and the lack of correlation between fluid mobile elements and Pb-isotope compositions (Churikova et al., 2001). Another three andesites are from Shiveluch volcano located at the northern termination of the Central Kamchatka Depression (NCKD) adjacent to the junction between the Kamchatka and Aleutian arcs (Fig. 1). They have 54.6–61.1 wt% SO_2 , 3.6–5.6 wt% MgO , 4.6–7.7 wt% FeO_{T} , and 99.8–134 ppm Zn (Fig. 2, Churikova et al., 2001). Their low $^{87}\text{Sr}/^{86}\text{Sr}$ (~0.703420), low $^{207}\text{Pb}/^{204}\text{Pb}$ (~15.48) and high ϵ_{Nd} (~10.0) rule out any significant addition of subducted sediments to the mantle wedge or shallow level crustal contamination (Churikova et al., 2001; Münker et al., 2004). Thus, their high Sr/Y ratios (33.3–54.5) (Fig. 3b) have been ascribed to addition of melts derived from oceanic crust to the mantle wedge (Churikova et al., 2001; Yogodzinski et al., 2001).

2.2. The Aleutian arc

The geological background of the Aleutian arc has been discussed extensively in the literature (e.g., Yogodzinski et al., 1995; Tibaldi and Bonali, 2017 and references therein). Briefly, the Aleutian arc is formed by subducting the Pacific plate beneath the American plate, and its northwesternmost part nearly perpendicularly meets the Kamchatka arc at ca. 57°N (Fig. 1). The Aleutian arc is sub-divided into the Western, Central, and Eastern

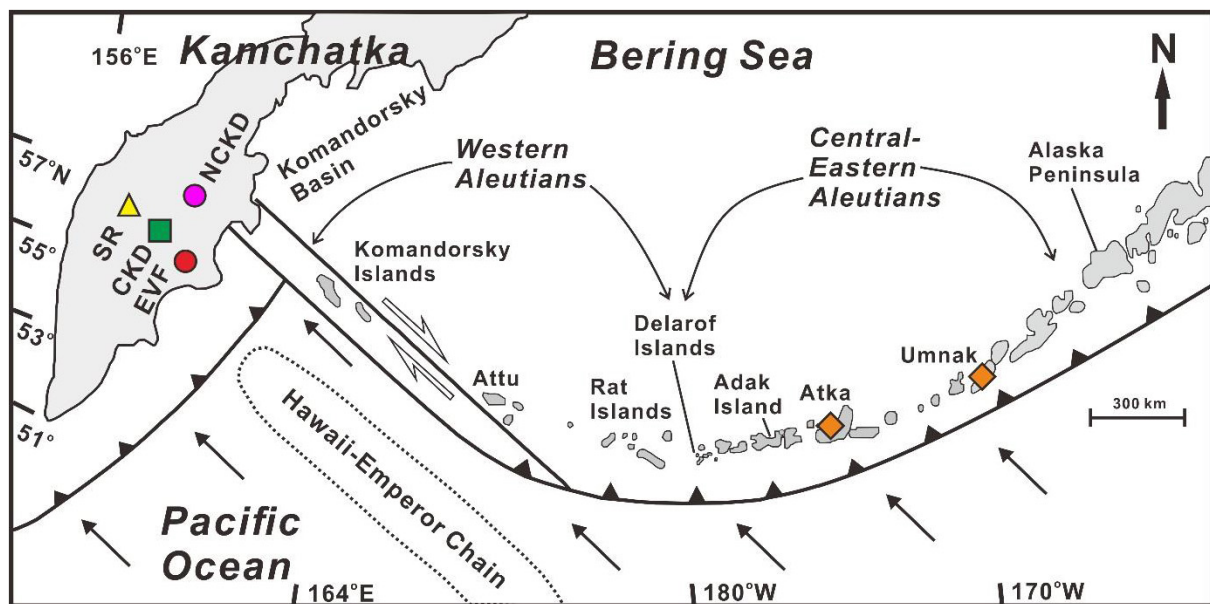


Fig. 1. Geological map of Kamchatka-Aleutian arcs with sample locations marked with color symbols, including EVF, CKD, SR, NCKD, Atka and Umnak. EVF = Eastern Volcanic Front, CKD = Central Kamchatka Depression, NCKD = Northern Central Kamchatka Depression, SR = Sredinny Ridge. Maps are modified from Münker et al. (2004) and Cai et al. (2015). (For interpretation of the references to colour in this figure legend, the reader is referred to the web version of this article.)

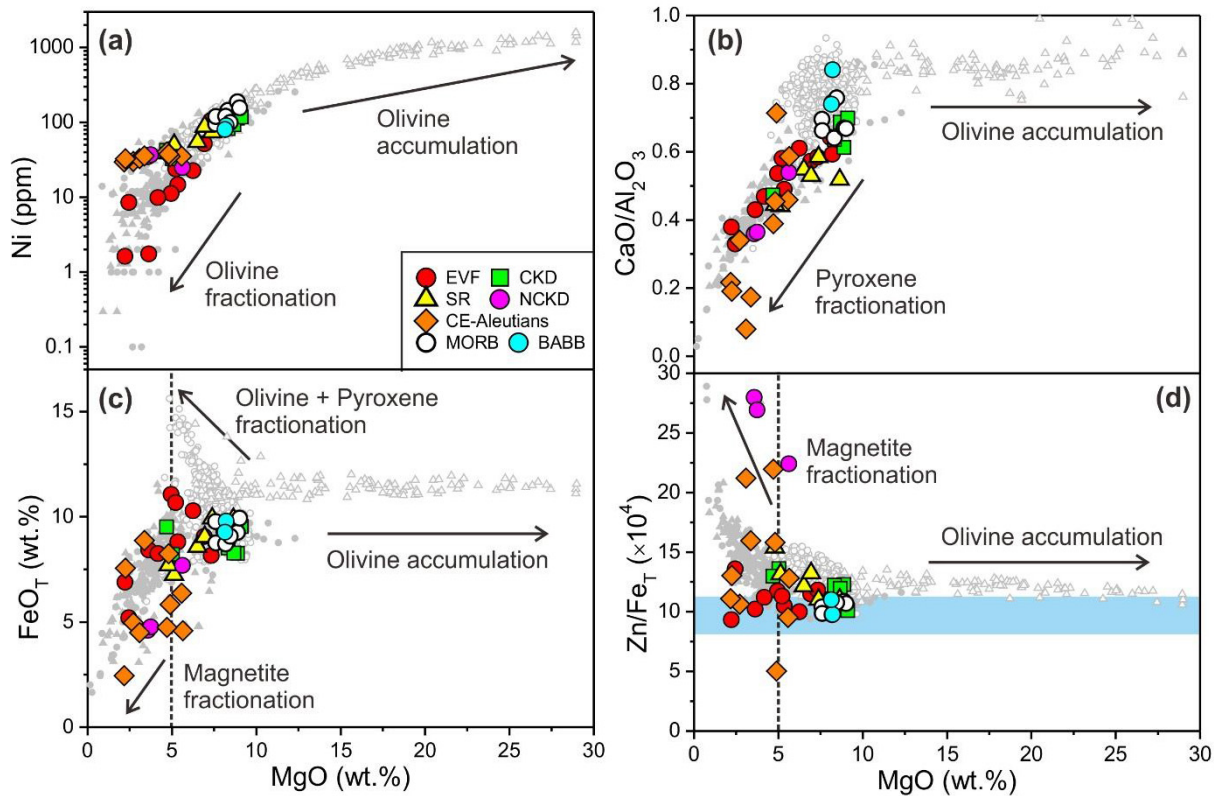


Fig. 2. Compositional variations of arc rocks, MORBs, and BABBs as MgO versus Ni (a), CaO/Al₂O₃ (b), FeOT (c), and Zn/FeOT ($\times 10^4$) (d). Data for samples (large symbols) studied here are from Churikova et al. (2001), Gale et al. (2013), and Cai et al. (2015). Small symbols denote a compilation for the Kamchatka (solid circles, Churikova et al., 2001) and Aleutian arc rocks (solid triangles, Yogodzinski et al., 2015), OIBs (open triangles, Hawaii Mauna Kea volcano, Huang and Frey, 2003) and MORBs (open circles, Jenner and O'Neill, 2012). The dashed lines in (c) and (d) denote the onset of magnetite fractionation in arc magmas (Lee et al., 2010).

segments (Yogodzinski et al., 1995; Cai et al., 2015). The Western Aleutians (west of 180°W) extends from the Komandorsky Islands to the eastern end of the Rat Islands, and the Central-Eastern (CE) Aleutians (east of 180°W) extends from the Delarof Islands to the western end of the Alaska Peninsula (Fig. 1) (Cai et al., 2015).

In the CE Aleutians, there are both intrusive and extrusive rocks. The calc-alkaline plutons have an Eocene to Miocene (39–9 Ma) age that are exposed below the younger Holocene tholeiitic lavas (Cai et al., 2015). Compared to the lavas, the plutonic rocks have negligible Eu anomalies, similar or higher Na₂O + K₂O and similar or lower CaO and Al₂O₃ at a given Mg#, suggesting that they represent magma compositions rather than crystal cumulates (Cai et al., 2015). Their major and trace element contents strongly resemble the calc-alkaline Holocene lavas with more depleted Sr-Nd-Pb-Hf isotope ratios in the Western Aleutians (Cai et al., 2015 and references therein). Specifically, the plutonic rocks from the CE Aleutians have high ϵ Nd (>6.3) and ϵ Hf (>11.8) coupled with higher Th/Nd and Hf/Lu compared to the DMM (Cai et al., 2015). These geochemical features have been ascribed to addition of low degree partial melts of subducted oceanic crust in eclogite facies, where residual omphacite and garnet preferentially

retain Nd and Lu relative to Th and Hf, respectively (e.g., Cai et al., 2014, 2015; Yogodzinski et al., 2015). This is consistent with their MORB-like ⁸⁷Sr/⁸⁶Sr and high Sr/Y (Fig. 3b, Cai et al., 2015).

The Aleutian samples examined here were calc-alkaline plutonic rocks from the Atka and Umnak islands in the CE Aleutians (Fig. 1). Their petrology, major and trace element contents, and Sr-Nd-Pb-Hf isotopic compositions have been previously reported (Cai et al., 2015). Our samples are basaltic to dacitic in compositions, including gabbro, diorite, and granodiorite. They have SiO₂ from 47.9 to 64.2 wt%, MgO from 2.2 to 5.6 wt%, FeOT from 4.4 to 8.9 wt%, and Zn from 21.1 to 110 ppm (Fig. 2, Cai et al., 2015). Together with the NCKD samples at Kamchatka, their Zn isotopic compositions therefore provide valuable insights into potential contributions to arc magmas from partial melting of subducted oceanic crust.

2.3. MORBs and BABBs

Mid-ocean ridge basalts were collected from zero-age centered ridge sections including the Gakkel Ridge at 84–87°N, the Mid-Atlantic Ridge at 37.1°E, and the Southeast Indian Ridge at 43–51°S. The spreading rates vary from

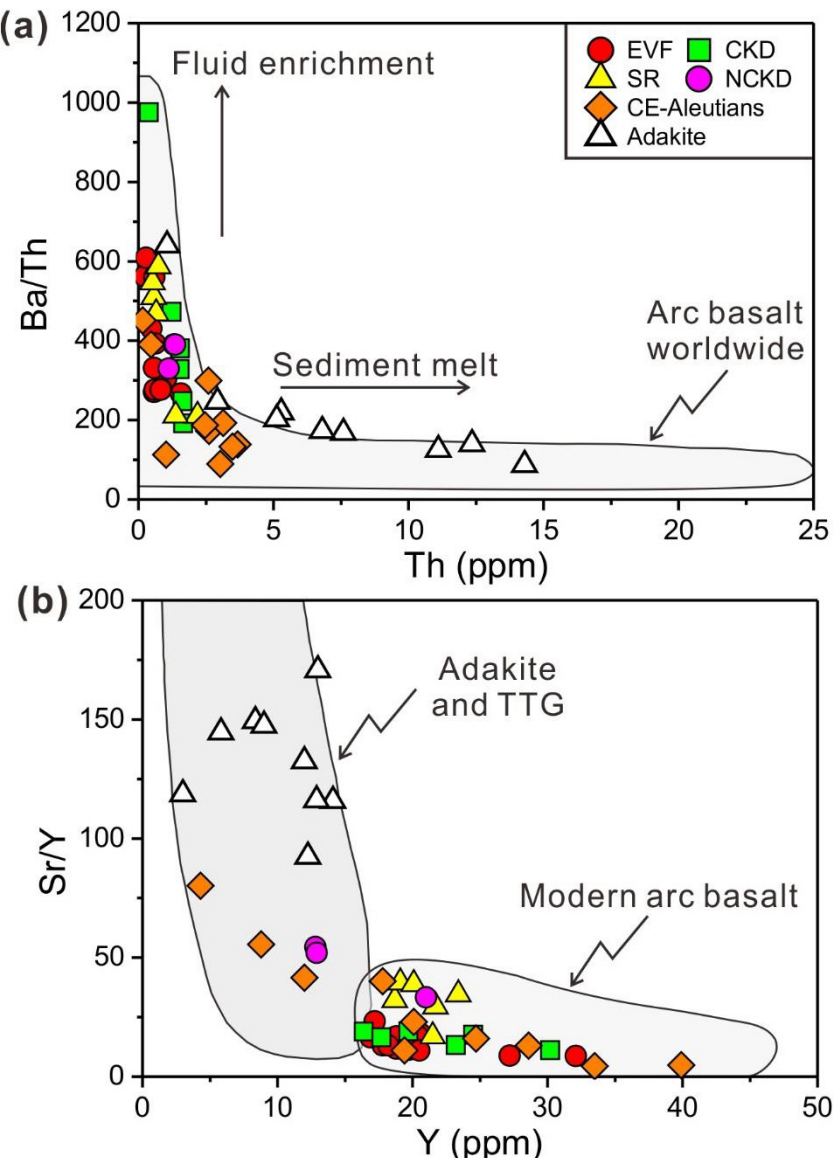


Fig. 3. Kamchatka-Aleutian arc rocks and adakites from the Central American Arc in comparison to other arc systems in Th versus Ba/Th (a) and Y versus Sr/Y (b). Data for Kamchatka-Aleutian arcs are from Churikova et al. (2001) and Cai et al. (2015), adakites from Abratis and Wörner (2001) and Wegner et al. (2011), and arc compilations from Drummond and Defant (1990) and Hawkesworth et al. (1997).

~10–13 cm/year for the Gakkel Ridge to ~55–72 cm/year for the Southeast Indian Ridge (Gale et al., 2013). These basalts have distinct compositions from normal (N) to enriched (E)-MORBs. Their major element compositions range from 7.58 to 9.01 wt% in MgO, from 0.85 to 2.08 wt% in TiO₂, from 0.04 to 0.32 wt% in K₂O, and from 0.04 to 0.23 in K₂O/TiO₂ ratios with (La/Sm)_{PM} from 0.42 to 1.12 (subscript PM indicates primitive mantle normalization) (Fig. 2, Bézos et al., 2009; Gale et al., 2013).

As a supplement to MORB samples, two BABBs from the Lau Basin (19–20°S) were also analyzed. The Lau Basin comprises part of the largest and fastest-spreading Lau-Fiji back-arc system with a spreading rate of ~90 cm/year (Gale et al., 2013). The studied BABBs have MgO contents of

~8.2 wt%, TiO₂ contents of ~0.90 wt%, and K₂O contents of ~0.05 wt% with K₂O/TiO₂ ratios of ~0.05 and (La/Sm)_{PM} of ~0.43 (Fig. 2, Gale et al., 2013).

2.4. Adakites

Nine adakites were analyzed from Costa Rica and Panama in the Central American Volcanic Arc that extends from western Guatemala to central Panama and formed by subducting the Cocos and Nazca plates beneath the Caribbean plate (Herrstrom et al., 1995). These adakites have ages of <2.0 Ma, SiO₂ contents of 53.8 to 68.4 wt%, MgO contents of 0.90–6.05 wt%, and Zn contents of 38.4–88.0 ppm (Table 2, Abratis and Wörner, 2001; Wegener et al.,

2011). They are thought to result from partial melting of the subducted AOC under eclogite-facies conditions, as manifested by their high Sr/Y (92.4–171, Fig. 3b) and La/Yb (22.7–56.5) ratios (Abratis and Wörner, 2001; Wegener et al., 2011) that are typical for adakitic melts from slab melting (Defant and Drummond, 1990). Therefore, these adakites offer an opportunity to assess the Zn isotopic feature of the AOC-derived melts, which can help us better understand the Zn isotopic data of the Kamchatka-Aleutian arc magmas.

3. ANALYTICAL METHODS

Zinc isotopes were analyzed at the Metal Stable Isotope Laboratory of the University of Science and Technology of China (USTC), China, following the procedures established by Chen et al. (2016). Sample powders were dissolved in Savillex beakers using double-distilled concentrated HF + HNO₃, HCl + HNO₃ and HCl successively. Separation of Zn was achieved by anion exchange chromatography with Bio-Rad AG-MP-1M strong anion resin in 0.5N HNO₃ media. The column chemistry was performed twice to efficiently purify Zn from matrix elements (e.g., Na, Mg, Al, K, Ti, V, Cr, Fe, Ni, and Cu). The Zn yields through column chemistry, based on analyses of Zn contents in the elution collected before and after the Zn cut, are ≥99.4%. The total procedural blanks (from sample dissolution to mass spectrometry) are from 2.1 to 3.0 ng (n = 2), negligible compared to ~2 µg Zn loaded on the resin.

Zinc isotope ratios were determined using a Thermo-Fisher *Neptune Plus* multi-collector inductively coupled mass spectrometry (MC-ICPMS) at the USTC. A sample-standard bracketing method without Cu doping was applied to correct instrumental mass bias and time drifts (Maréchal et al., 1999; Chen et al., 2016). Five Zn isotopes (64, 66, 67, 68, and 70) were collected by L2, C, H1, H3, and H4 cups, respectively. A Ni(X) + Ni (Jet) cone assembly was used with the ⁶⁴Zn sensitivity of ca. 25 V/ppm at low mass resolution conditions. Zinc isotope ratios are reported in standard δ-notation in per mil relative to Zn standard JMC Lyon 3-0749L: $\delta^X\text{Zn} = [({}^X\text{Zn}/{}^{64}\text{Zn})_{\text{sample}}/({}^X\text{Zn}/{}^{64}\text{Zn})_{\text{JMC Lyon 3-0749L}} - 1] \times 1000 (\text{\textperthousand})$, where X = 66, 67, 68, or 70. During the course of this study, repeated analyses of IRMM3702 yielded $\delta^{66}\text{Zn}$ of $0.27 \pm 0.05\text{\textperthousand}$ (2SD, n = 51, Table S1), consistent with that of a previous study ($0.29 \pm 0.05\text{\textperthousand}$, 2SD, Moeller et al., 2012). The long-term external reproducibility for $\delta^{66}\text{Zn}$ is $\pm 0.05\text{\textperthousand}$ (2SD) for this study. Six international whole rock standards (i.e., AGV-2, BHVO-2, BCR-2, BIR-1, GSP-1, and W-2) were processed through column chemistry together with samples for accuracy checks. Their $\delta^{66}\text{Zn}$ values agree well with previously published values within error (see the detailed compilation of previous and our values in Table S1). This, combined with consistent results for repeated analyses (Table 1), assures the accuracy and precision of our data.

Supplementary data associated with this article can be found, in the online version, at <https://doi.org/10.1016/j.gca.2018.07.012>.

4. RESULTS

Zinc isotopic compositions of the Kamchatka-Aleutian arc rocks, MORBs, BABBs, and adakites are listed in Tables 1 and 2, respectively. In a plot of $\delta^{66}\text{Zn}$ versus $\delta^{68}\text{Zn}$ (Fig. 4), our data fall on the theoretical mass-dependent line of slope 1.94 (i.e., $\delta^{68}\text{Zn} \approx 1.94 \times \delta^{66}\text{Zn}$, Schauble, 2004), indicating that Zn isotopes obey the mass-dependent fractionation law. Thus, we only discuss the $\delta^{66}\text{Zn}$ values in this study. Rocks from the Kamchatka and CE Aleutian arcs have a total range in $\delta^{66}\text{Zn}$ from 0.16 to 0.31‰. There are no systematic differences in $\delta^{66}\text{Zn}$ among the samples that are dominantly affected by (1) slab-derived fluids (e.g., EVF, CKD, and SR in Kamchatka) and (2) oceanic crust-derived melts (e.g., NCKD in Kamchatka, Atka and Umnak in CE Aleutians) (Fig. 5). The average $\delta^{66}\text{Zn}$ are $0.23 \pm 0.04\text{\textperthousand}$ for EVF rocks (2SD, N = 12), $0.23 \pm 0.05\text{\textperthousand}$ (2SD, N = 6) for CKD rocks, $0.26 \pm 0.07\text{\textperthousand}$ (2SD, N = 6) for SR rocks, and $0.24 \pm 0.07\text{\textperthousand}$ (2SD, N = 3) for NCKD rocks in the Kamchatka arc. Rocks from the CE-Aleutian arc have an average $\delta^{66}\text{Zn}$ of $0.24 \pm 0.10\text{\textperthousand}$ (2SD, N = 10). These values are similar to those of MORBs (0.21–0.31‰ with an average of $0.27 \pm 0.05\text{\textperthousand}$, 2SD, N = 13) reported in Wang et al. (2017) and this study. Because melt extraction has a negligible effect on the Zn isotopic composition of the mantle residue, the $\delta^{66}\text{Zn}$ of the DMM should be identical to that of the PM ($0.16 \pm 0.06\text{\textperthousand}$, Sossi et al., 2018). Relative to the DMM, many arc lavas, but also MORBs show statistically higher $\delta^{66}\text{Zn}$ (Fig. 5).

Two BABBs from the Lau Basin have an identical $\delta^{66}\text{Zn}$ of ~0.25‰, and nine adakites from the Central American Volcanic Arc have $\delta^{66}\text{Zn}$ from 0.23 to 0.33‰ (Fig. 5).

5. DISCUSSION

5.1. The influence of fractional crystallization

Based on a systematic study of chemically differentiated, cogenetic igneous rocks from the Kilauea Iki lava lake, Hawaii, Chen et al. (2013) found that the $\delta^{66}\text{Zn}$ values show a negative correlation with MgO contents (Fig. 5a) and positive correlations with SiO₂ and Zn contents. This indicates Zn isotope fractionation during magma differentiation with the evolved melts exhibiting ⁶⁶Zn enrichment. In the Kilauea Iki lava lake, the chemical compositions of rocks with MgO > ~11 wt% were affected by various extents of olivine accumulation (Helz, 1987, 2009). Their $\delta^{66}\text{Zn}$ values decrease with increasing MgO contents (Fig. 5a), suggesting that olivine is enriched in ⁶⁴Zn relative to basaltic melts, consistent with direct measurements on olivine ($\delta^{66}\text{Zn} \approx 0.15\text{\textperthousand}$) that is isotopically lighter compared to basaltic rocks ($\delta^{66}\text{Zn} \approx 0.25\text{\textperthousand}$) (Sossi et al., 2015; Wang et al., 2017). However, the increasing $\delta^{66}\text{Zn}$ in rocks with MgO < 5 wt% (Fig. 5a) cannot be explained by fractionation of olivine (Chen et al., 2013) because it stops forming below ~6.5 wt% MgO (Helz, 1987). Instead, Fe-Ti oxide fractionation starts at MgO ≈ 5 wt% (Helz, 1987, 2009) and contributes to the elevated $\delta^{66}\text{Zn}$ of the highly evolved melts in the Kilauea Iki lava lake (Chen et al., 2013). Such rocks

Table 1
Zinc and its isotopic compositions and selected major element contents of the Kamchatka-Aleutian arc magmas.

Location	Sample	Rock ^a type	DTT ^b km	SiO ₂ ^c wt.%	MgO ^c wt.%	FeO _T ^c wt.%	Zn ^c ppm	δ ⁶⁶ Zn ^d ‰	2SD ^e	δ ⁶⁸ Zn ^d ‰	2SD ^e	N ^f
Kamchatka												
EVF	GAM-07	B	200	51.6	5.4	8.8	72.0	0.24	0.01	0.45	0.12	3
EVF	GAM-14	BA	200	55.8	3.6	8.4	67.0	0.23	0.01	0.47	0.01	3
EVF	GAM-26	B	200	50.6	4.9	11.1	101	0.22	0.01	0.46	0.02	3
EVF	GAM-28	B	200	49.8	6.2	10.3	80.0	0.21	0.02	0.38	0.07	3
EVF	KIZ-01/1	D	230	63.6	2.4	5.2	55.0	0.21	0.06	0.40	0.10	3
EVF	KIZ-19	B	230	50.3	5.2	10.7	94.0	0.19	0.02	0.37	0.02	3
EVF	KIZ-24	BA	230	54.7	4.2	8.3	72.0	0.26	0.05	0.53	0.07	3
EVF	SHM-01	B	198	50.6	8.1	9.3	78.0	0.26	0.05	0.48	0.03	3
EVF	SHM-03	A	198	59.1	2.2	6.9	50.0	0.22	0.02	0.47	0.02	3
EVF	SHM-04	B	198	50.9	6.9	9.1	81.0	0.23	0.05	0.49	0.09	6
	Replicate ^g							0.25	0.02	0.49	0.02	3
EVF	KOM-02/2	BA	202	53.7	7.3	8.2	75.0	0.24	0.04	0.48	0.06	6
EVF	KOM-06	B	202	51.7	8.2	9.3	81.0	0.22	0.04	0.44	0.05	6
CKD	KLU-03	B	280	53.7	8.9	8.3	79.0	0.24	0.02	0.50	0.25	3
CKD	KLU-06	B	280	53.5	8.3	8.5	81.0	0.20	0.02	0.41	0.03	3
CKD	KLU-12	B	280	54.0	5.0	8.2	87.0	0.21	0.04	0.44	0.08	3
	Replicate ^g							0.27	0.02	0.53	0.01	3
CKD	KLU-15	B	280	53.4	8.7	8.3	77.0	0.22	0.05	0.44	0.10	6
CKD	TOL-96-01	B	275	52.1	4.7	9.5	96.3	0.27	0.04	0.54	0.07	6
CKD	TOL-96-03	B	275	50.9	9.1	9.5	74.9	0.25	0.04	0.49	0.09	3
SR	ESO-08	B	375	50.6	6.5	8.6	81.0	0.23	0.06	0.47	0.13	3
SR	ACH-01	A	335	54.4	5.1	7.2	74.0	0.22	0.04	0.46	0.05	6
SR	ICH-02	A	400	54.9	4.8	7.7	92.0	0.23	0.06	0.46	0.11	3
SR	ICH-05	B	400	47.4	7.4	9.9	85.0	0.31	0.04	0.61	0.07	6
	Replicate ^g							0.31	0.04	0.65	0.12	6
SR	ICH-10	B	400	47.8	8.6	9.9	85.0	0.29	0.05	0.60	0.06	6
SR	ICH-69	B	400	50.5	6.9	9.0	93.0	0.25	0.04	0.52	0.06	6
NCKD	SHIV-01-01	A	200	61.2	3.6	4.6	100	0.24	0.02	0.51	0.01	3
NCKD	SHIV-01-05	A	200	54.6	5.6	7.7	134	0.20	0.02	0.41	0.03	3
NCKD	SHIV-01-12	A	200	61.1	3.7	4.8	99.8	0.28	0.01	0.57	0.02	3
CE Aleutians												
Atka	877-7-2	G	ND	47.9	5.6	4.6	45.7	0.19	0.05	0.36	0.03	3
Atka	877-12-8	Dt	ND	53.6	5.6	6.4	47.2	0.31	0.03	0.65	0.05	3
Atka	877-14-5II	Dt	ND	59.0	4.7	4.7	81.0	0.16	0.03	0.33	0.06	3
Atka	877-15-1'	Dt	ND	55.1	4.9	5.8	22.7	0.29	0.01	0.60	0.01	3
Atka	877-15-4	Dt	ND	58.8	2.7	5.0	41.1	0.29	0.04	0.56	0.10	3
Atka	877-16-6	GD	ND	64.2	2.2	2.4	21.1	0.28	0.00	0.53	0.04	3
Umnak	47ABy3	Dt	ND	60.1	3.1	4.5	74.0	0.22	0.04	0.47	0.07	3
Umnak	47ABy31	A	ND	60.5	3.4	8.9	110	0.22	0.03	0.48	0.01	3
Umnak	47ABy34	Dt	ND	61.9	2.2	7.6	76.5	0.27	0.04	0.56	0.09	3
Umnak	47ABy41	Dt	ND	55.4	4.8	8.2	101	0.21	0.02	0.45	0.02	3

^a A = Andesite, B = Basalt, BA = Basaltic andesite, D = Dacite, G = Gabbro, GD = Granodiorite, Dt = Diorite.

^b DTT = Distance to trench, ND = Not Available.

^c Data for SiO₂, MgO, FeO_T and Zn are taken from Churikova et al. (2001) and Cai et al. (2015).

^d δ^XZn (‰) = [(^XZn/⁶⁴Zn)_{sample}/(^XZn/⁶⁴Zn)_{JMC Lyon 3072} - 1] × 1000, where X = 66 or 68 and JMC Lyon 3072 is an international Zn isotope-normalized standard.

^e 2SD = two times the standard deviation of the population of n repeated measurements of the same solution.

^f N represents the times of repeat measurements of the same purified solution by MC-ICP-MS.

^g Replicate = repeated the whole procedure, including sample dissolution, column chemistry and mass spectrometry.

Table 2
Zinc and its isotopic compositions and selected major and trace element contents of MORBs, BABBs, and adakites.

Sample	Segments	Type	SiO ₂ ^a (wt.%)	MgO ^a (wt.%)	(La/Sm) _{PM} ^a	Zn ^a (ppm)	δ ⁶⁶ Zn ^b (‰)	2SD ^c	δ ⁶⁸ Zn ^b (‰)	2SD ^c	N ^d
Gakkel Ridge											
HLY0102-023-027	GAKK16	N-MORB	50.3	7.58	0.76	76.1	0.27	0.03	0.54	0.10	3
HLY0102-038-029	GAKK13	E-MORB	50.8	8.80	1.12	67.2	0.26	0.01	0.54	0.04	3
HLY0102-053-21	GAKK10	N-MORB	49.2	8.31	0.94	74.5	0.30	0.02	0.58	0.05	3
Mid-Atlantic Ridge											
AII0127 D7-2	MARR92	N-MORB	52.3	8.88	0.53	77.6	0.21	0.03	0.43	0.05	3
South East Indian Ridge											
VEM0033-1-001-002	SEIR69	E-MORB	48.8	9.01	1.04	82.6	0.31	0.01	0.60	0.08	3
VEM0033-1-005-005	SEIR67	N-MORB	50.6	8.69	0.59	66.1	0.25	0.02	0.50	0.04	3
VEM0033-1-003-004	SEIR70	N-MORB	49.5	8.45	0.78	75.9	0.24	0.02	0.50	0.04	3
Lau Basin (BABBs)											
KLM0417-005-001	BLAU7	Basalt	51.0	8.21	0.42	73.4	0.25	0.04	0.48	0.09	3
KLM0417-007-001	BLAU7	Basalt	49.1	8.14	0.45	98.8	0.25	0.03	0.47	0.04	3
Replicate ^e							0.24	0.05	0.45	0.08	3
Central America Arc											
ALT-60	Costa Rica	Adakite	53.8	6.05		74.5	0.31	0.02	0.62	0.08	3
ALT-63	Costa Rica	Adakite	57.7	3.75		68.0	0.29	0.03	0.61	0.04	3
VIT-54	Costa Rica	Adakite	55.4	4.96		78.0	0.33	0.04	0.62	0.11	3
PAN-06-165	Panama	Adakite	59.7	2.93		66.9	0.26	0.03	0.48	0.01	3
PAN-06-177	Panama	Adakite	57.0	3.30		72.2	0.25	0.00	0.50	0.06	3
PAN-06-043	Panama	Adakite	62.9	1.23		50.0	0.28	0.02	0.54	0.02	3
PAN-05-047	Panama	Adakite	68.4	0.90		38.4	0.30	0.01	0.61	0.07	3
PAN-06-014	Panama	Adakite	55.6	3.21		82.0	0.23	0.01	0.44	0.08	3
PAN-06-006	Panama	Adakite	59.4	3.30		88.0	0.28	0.03	0.54	0.05	3

^a Major and trace element contents for MORBs and BABBs are taken from Gale et al. (2013) and for adakites from Abratis and Wörner (2001) and Wegner et al., 2011). Subscript PM in (La/Sm)_{PM} denotes Primitive Mantle-normalization.

^b δ^XZn (‰) = [(^XZn/⁶⁴Zn)_{sample}/(^XZn/⁶⁴Zn)_{JMC Lyon 3072} – 1] × 1000, where X = 66 or 68 and JMC Lyon 3072 is an international Zn isotope-normalized standard.

^c 2SD = two times the standard deviation of the population of n repeated measurements of the same solution.

^d N represents the times of repeat measurements of the same purified solution by MC-ICP-MS.

^e Replicate = repeated the whole procedure, including sample dissolution, column chemistry and mass spectrometry.

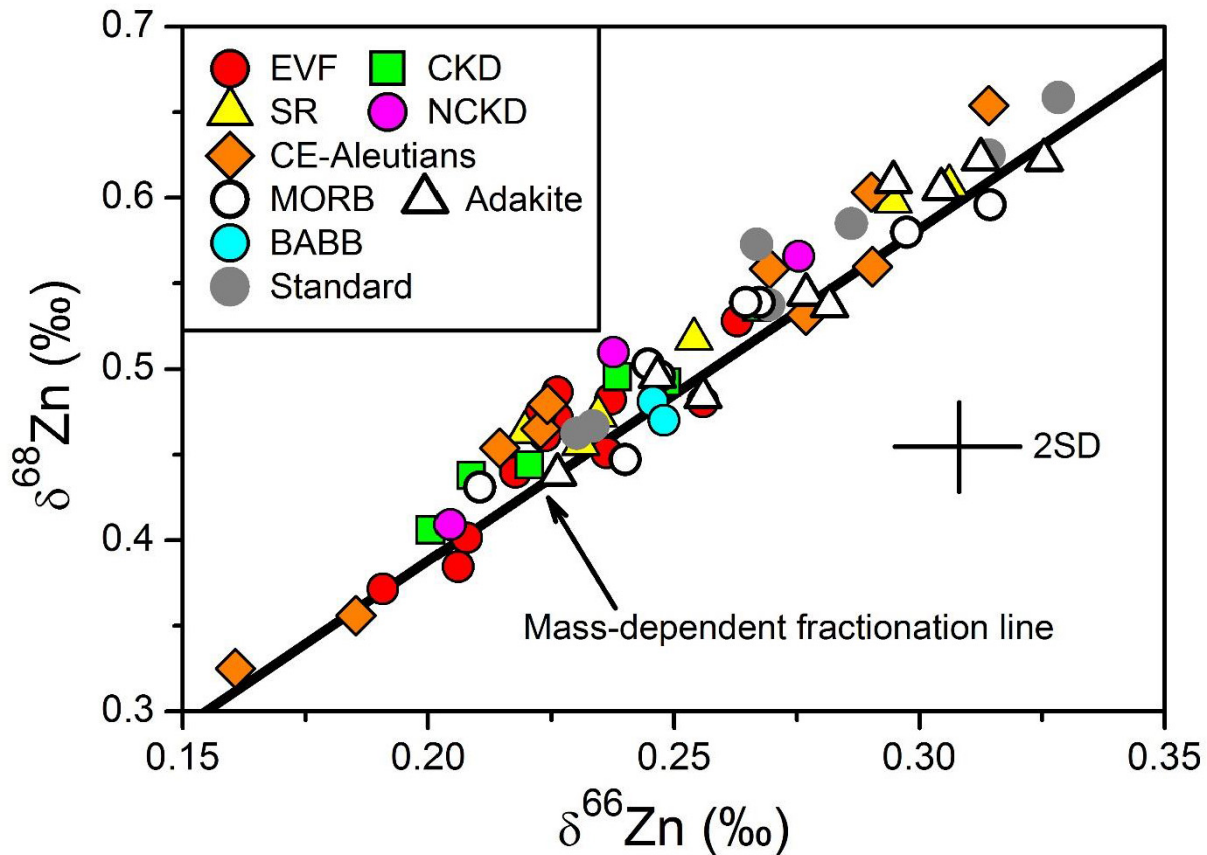


Fig. 4. Three Zn isotope diagram for samples and standards analyzed in this study. All data fall on the theoretical mass-dependent fractionation line of slope 1.94 (Schauble, 2004). 2SD = $2 \times$ Standard Deviation.

with MgO < 5 wt% also have the heaviest Fe isotopic compositions (Teng et al., 2008), suggesting that the segregated Fe-Ti oxides predominantly consist of ilmenite rather than magnetite because the former is enriched and the latter is depleted in the light Fe isotopes relative to melts (Du et al., 2017 and references therein).

Determined Zn/Fe exchange coefficients between minerals and melts ($K_{D(\text{mineral}/\text{melt})}^{\text{Zn/Fe}}$) are ~0.9–1 for olivine, ~0.6 for clinopyroxene, 0.2 for ilmenite, and 0.5 for magnetite (Ewart and Griffin, 1994; Le Roux et al., 2010), suggesting that olivine fractionation has a limited influences on Zn/Fe_T of the residual melts but fractionation of clinopyroxene, ilmenite and magnetite fractionation may cause an increase in Zn/Fe_T. Major and trace element variations indicate that magmas in the Hekla volcano (Iceland) underwent extensive titanomagnetite fractionation during differentiation (Schuessler et al., 2009). However, variably evolved Hekla magmas (SiO₂ < 55 wt% to >67 wt%) all have identical Zn isotopic compositions within analytical uncertainties ($\pm 0.04\text{\textperthousand}$), indicating that magnetite fractionation has an insignificant effect on δ⁶⁶Zn of the highly evolved melts (Chen et al., 2013). Thus, only ilmenite fractionation is likely to cause the positive correlation between δ⁶⁶Zn and Zn/Fe_T in the highly differentiated lavas of the Kilauea Iki (Fig. 5c).

Our results for the Kamchatka and CE Aleutian arc rocks do not show correlations of δ⁶⁶Zn with MgO and Zn/Fe_T (Fig. 5b, d), suggesting that fractional crystallization of olivine, clinopyroxene and magnetite cause limited variations in δ⁶⁶Zn of subduction-related magmas at convergent plate margins. This is further supported by the constant δ⁶⁶Zn of mafic to highly evolved rocks from the EVF in the Kamchatka arc (Fig. 6a). Thus, we conclude that magma differentiation has no significant effect on the Zn isotopic compositions of the studied Kamchatka and CE Aleutian arc rocks.

5.2. The influence of subduction components

Geochemical characteristics of arc magmas reflect incorporation of subduction components to their mantle wedge sources in subduction zones (e.g., Pearce and Peate, 1995; Kelemen et al., 2007). The first systematic Zn isotopic data for arc rocks presented here allow us to assess the effect of subduction components on the Zn isotopic budget of arc magmas.

5.2.1. Oceanic crust-derived fluids

Barium/thorium and barium/lanthanum ratios have been widely used to trace slab-fluid enrichment, as Ba is

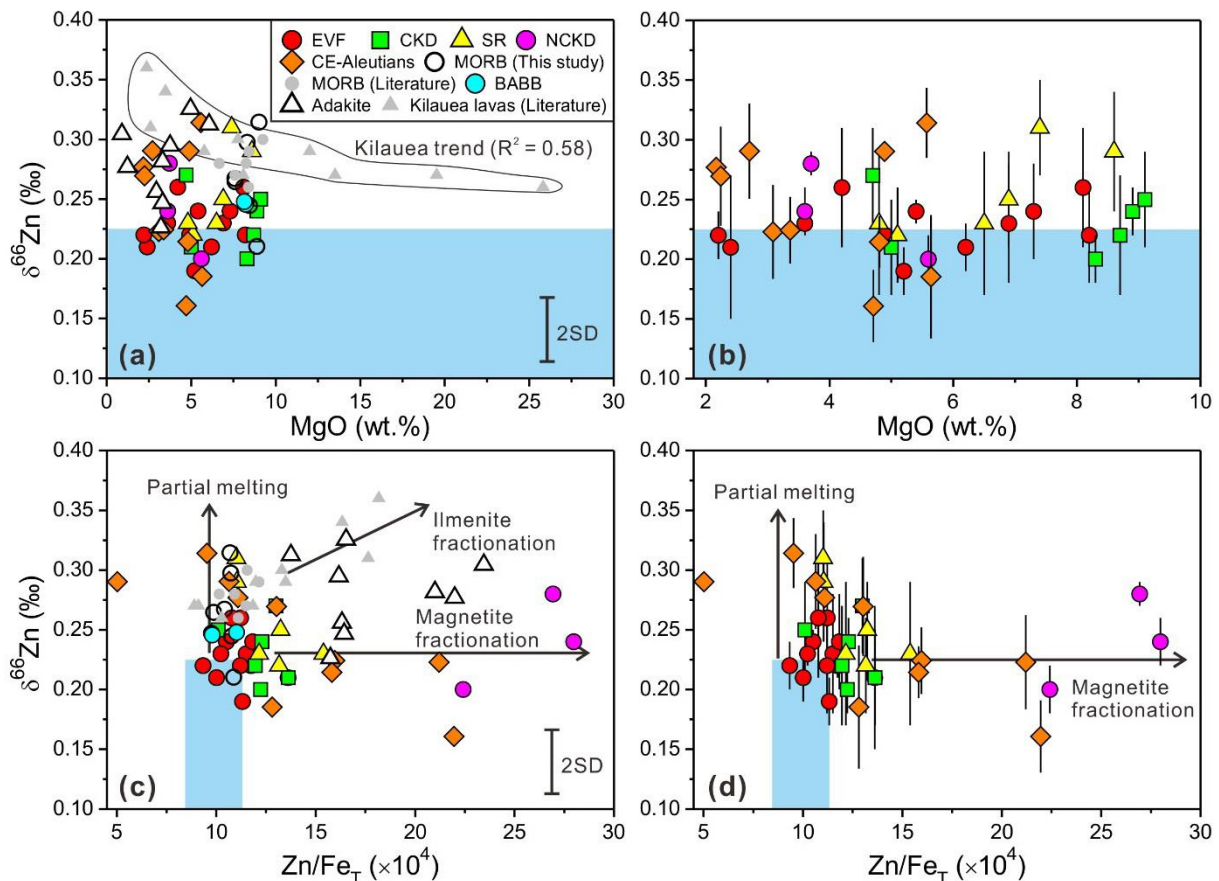


Fig. 5. $\delta^{66}\text{Zn}$ versus MgO and $\text{Zn}/\text{Fe}_T \times 10^4$ for all samples (a, c) and only Kamchatka-Aleutian arc rocks (b, d). Literature Zn isotopic data for MORBs (Wang et al., 2017) and Hawaii Kilauea lavas (Chen et al., 2013). Sources for major and trace element data are the same as in Fig. 2. Blue bars define the range of $\delta^{66}\text{Zn}$ (Sossi et al., 2018) and Zn/Fe_T (Lee et al., 2010) for the normal mantle. (For interpretation of the references to color in this figure legend, the reader is referred to the web version of this article.)

more mobile than Th and La in fluids but their compatibilities are generally similar during mantle melting (Kogiso et al., 1997; Arevalo and McDonough, 2010). In Ba/Th versus Th space (Fig. 3a), the EVF + CKD + SR rocks in Kamchatka cover the whole compositional range of fluid-dominated intra-oceanic arcs and thus represent an end member for a fluid-dominated sub-arc mantle regime (Churikova et al., 2001; Münker et al., 2004). Their Sr-Pb-O isotopic compositions reveal that the fluids are predominantly derived from the Pacific AOC (Dorendorf et al., 2000; Churikova et al., 2001). Measurements of melt inclusions hosted in olivine phenocrysts indicates that the AOC-derived fluids in the front-arc EVF are enriched in B, Cl, F, S, LILE (e.g., U, Th, Ba, and Pb), and LREE (La and Ce), in the CKD are enriched in S and U, and in the back-arc SR are enriched in F, Li, Be, LILE, and LREE (Churikova et al., 2007). If the AOC-derived fluids had a significant contribution to the Zn isotopic budget of the Kamchatka arc rocks, then their $\delta^{66}\text{Zn}$ should co-vary with the established fluid tracers (e.g., Ba/Th and Ba/La). However, no co-variations are observed between $\delta^{66}\text{Zn}$ and element ratios that characterize slab-derived fluids (e.g., Ba/Th and Ba/La, Fig. 7a, b). There is also no correlation of $\delta^{66}\text{Zn}$ with Sr isotopic compositions

(Fig. 8). In addition, potential mixing trajectories between AOC-derived fluids and the DMM deviate significantly from the regimes defined by our arc rocks in the plot of $\delta^{66}\text{Zn}$ versus $^{87}\text{Sr}/^{86}\text{Sr}$ (Fig. 8). Furthermore, there is no systematic variation in $\delta^{66}\text{Zn}$ of the EVF + CKD + SR rocks along the 56° arc traverse from trench to back arc (Fig. 6b). Finally, the average $\delta^{66}\text{Zn}$ of the Kamchatka rocks ($0.24 \pm 0.06\text{‰}$, 2SD) is indistinguishable from that of MORBs ($0.27 \pm 0.05\text{‰}$, 2SD, Wang et al., 2017; this study). Thus, we conclude that addition of fluids derived from the subducted AOC has an insignificant effect on the Zn isotopic budget of the mantle wedge in Kamchatka and CE-Aleutians. This is consistent with the observation that no detectable Zn isotope fractionation occurs during dehydration of basaltic oceanic crust because only a small proportion of the total Zn is extracted from the subducted mafic lithologies by fluids (Inglis et al., 2017).

5.2.2. Oceanic crust-derived melts

Bentahila et al. (2008) reported that one andesite from Taiwan Island has $\delta^{66}\text{Zn}$ up to $0.55 \pm 0.05\text{‰}$. Such a heavy Zn isotopic signature was attributed to (1) the particular Zn isotopic characteristics of Taiwan rocks, since Taiwan sedimentary rocks (e.g., pelites) also have heavy Zn isotopic

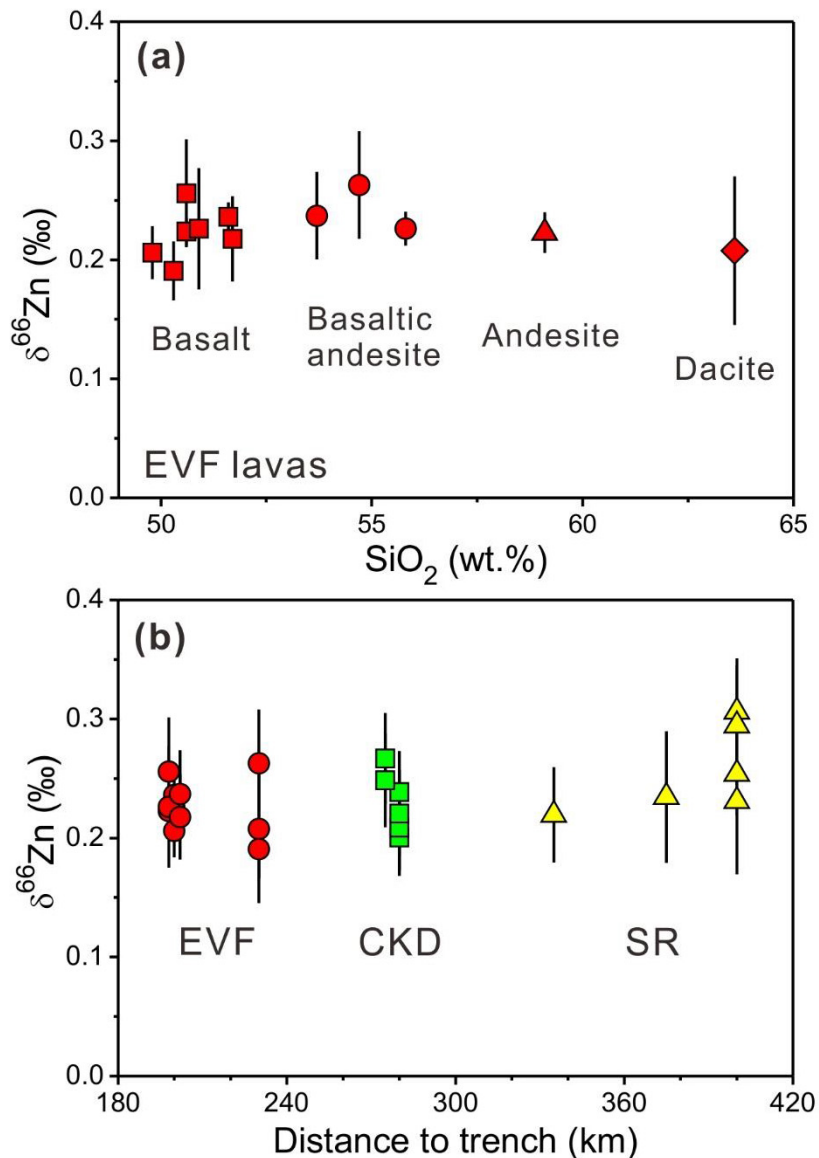


Fig. 6. (a) $\delta^{66}\text{Zn}$ versus SiO_2 in EVF rocks and (b) $\delta^{66}\text{Zn}$ in arc rocks along an traverse in Kamchatka. Distance to trench and SiO_2 contents are from Churikova et al. (2001).

compositions ($\delta^{66}\text{Zn}$ up to $0.48 \pm 0.05\text{\textperthousand}$) and thus being not representative at a global scale or (2) incorporation of slab melts derived from partial melting of the AOC that is assumed to have particularly high $\delta^{66}\text{Zn}$ (Bentahila et al., 2008). However, direct Zn isotopic measurements of altered basalts and gabbros recovered from IODP Site 1256 at the East Pacific Rise showed that the AOC in fact has an MORB-like average $\delta^{66}\text{Zn}$ of $\sim 0.27\text{\textperthousand}$ (Huang et al., 2016). In addition, the studied adakites, thought to represent partial melts of the subducted AOC (Abratis and Wörner, 2001; Wegner et al., 2011), have $\delta^{66}\text{Zn}$ of $0.23\text{--}0.33\text{\textperthousand}$ (Table 2). The $\delta^{66}\text{Zn}$ of both the AOC and its derivative melts are lower than that of the Taiwan andesite and thus inconsistent with the second interpretation of Bentahila et al. (2008).

Strontium/yttrium and hafnium/lutetium can be used as sensitive tracers of partial melts of the subducted AOC in

eclogite facies, where garnet preferentially retains Lu and Y compared to Hf and Sr, leading to higher Sr/Y and Hf/Lu in the AOC-derived melts than in the DMM (e.g., Kay, 1978; Defant and Drummond, 1990; Cai et al., 2015). The NCKD rocks from the Shiveluch volcano in Kamchatka have higher Sm/Yb and Sr/Y ratios (Fig. 3b) than those of the EVF + CKD + SR rocks from the fluid-dominated mantle sources. Such a pattern is typical for adakites, which are thought to be derived from slab melting (Kay, 1978; Defant and Drummond, 1990). In addition, an alkali-rich adakitic component in the NCKD lavas is manifested by their unusually high $(\text{SiO}_2)_{6.0}$, $(\text{K}_2\text{O})_{6.0}$ and $(\text{Na}_2\text{O})_{6.0}$ values (subscript 6.0 indicates normalization to 6 wt% MgO, Churikova et al., 2001). The NCKD volcanoes are located directly along the extension of the subducted transform boundary between the Pacific and Komandorsky plates (Fig. 1). Here, the Pacific plate is torn, surrounded,

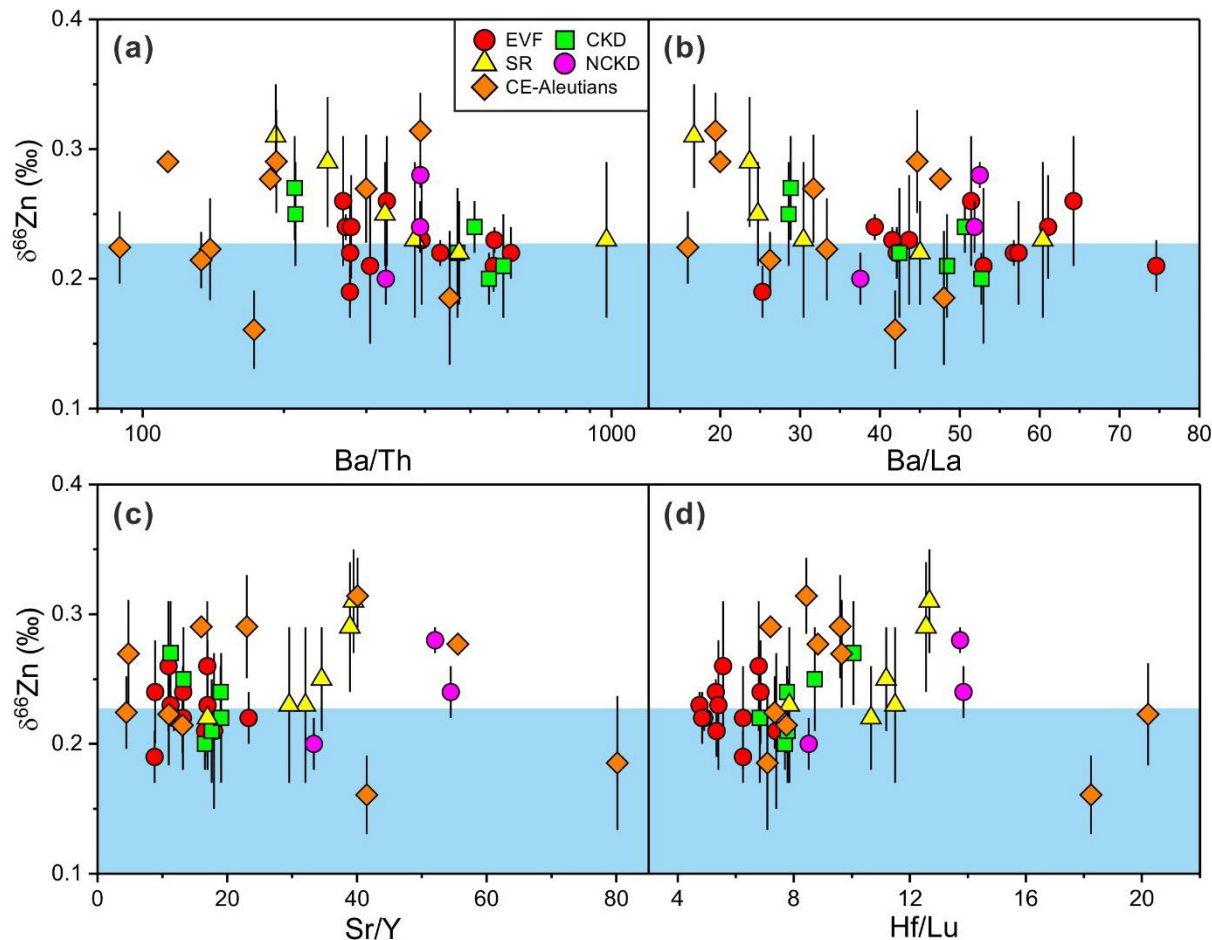


Fig. 7. $\delta^{66}\text{Zn}$ versus Ba/Th (a), Ba/La (b), Sr/Y (c), and Hf/Lu (d) in the Kamchatka and Aleutian arc rocks. Trace element abundance data are from Churikova et al. (2001), Münker et al. (2004), and Cai et al. (2015). Blue bars define the range of $\delta^{66}\text{Zn}$ for the normal mantle (Sossi et al., 2018). (For interpretation of the references to color in this figure legend, the reader is referred to the web version of this article.)

and heated by hot convecting mantle, and it partially melts to generate adakitic magmas which become a component in arc magmas erupted in this region (Yogodzinski et al., 2001).

The AOC-derived melts may also be involved in the petrogenesis of the Eocene to Miocene (~ 9 –39 Ma) plutonic rocks from the Atka and Umnak islands in the CE-Aleutians (Cai et al., 2015). These rocks display high ϵNd (>6.3) and ϵHf (>12.1) with higher Th/Nd and Hf/Lu than the DMM source for MORBs (Salter and Stracke, 2004). Such geochemical features are consistent with significant contributions from melts of subducted AOC at eclogite facies, where omphacite and garnet preferentially retain Nd and Lu in the solid residues compared to Th and Hf (Cai et al., 2014, 2015; Yogodzinski et al., 2015). In the plots of ϵNd versus Th/Nd and ϵHf versus Hf/Lu, mixing models indicate that at most 10% AOC-derived melts were added to the mantle sources of the CE-Aleutian plutons (Cai et al., 2015). The AOC-derived melts, represented by the adakites investigated here (Table 2), have an average $\delta^{66}\text{Zn}$ of $0.28\text{\textperthousand}$ and Zn content of 68.7 ppm. Incorporation of 10% such adakitic melts could only increase the DMM $\delta^{66}\text{Zn}$ from $0.16\text{\textperthousand}$ (Sossi et al., 2018) to $0.17\text{\textperthousand}$ (Fig. 8).

This, together with the lack of correlations of $\delta^{66}\text{Zn}$ with Sr/Y and Hf/Lu (Fig. 7c,d), suggests that the AOC-derived slab melts play a minor role in modifying the Zn isotopic budget of the Kamchatka-Aleutian arc magmas.

Collectively, recycling of oceanic crust in the subducting oceanic lithosphere cannot significantly modify the $\delta^{66}\text{Zn}$ of the mantle wedge sources for magmas from the Kamchatka and CE-Aleutian arcs.

5.3. The influence of mantle melting

Since the high $\delta^{66}\text{Zn}$ of most Kamchatka and CE-Aleutian arc rocks (Fig. 5) cannot be attributed to crystal fractionation during magma differentiation or the incorporation of subduction components into the mantle wedge sources, mantle partial melting offers a plausible explanation for the Zn isotopic discrepancies between the DMM and arc magmas investigated here. A measurable Zn isotope fractionation during mantle melting has been previously proposed to explain the heavier Zn isotopic compositions of MORBs and OIBs compared to the normal mantle (Doucet et al., 2016; Wang et al., 2017; Sossi et al., 2018).

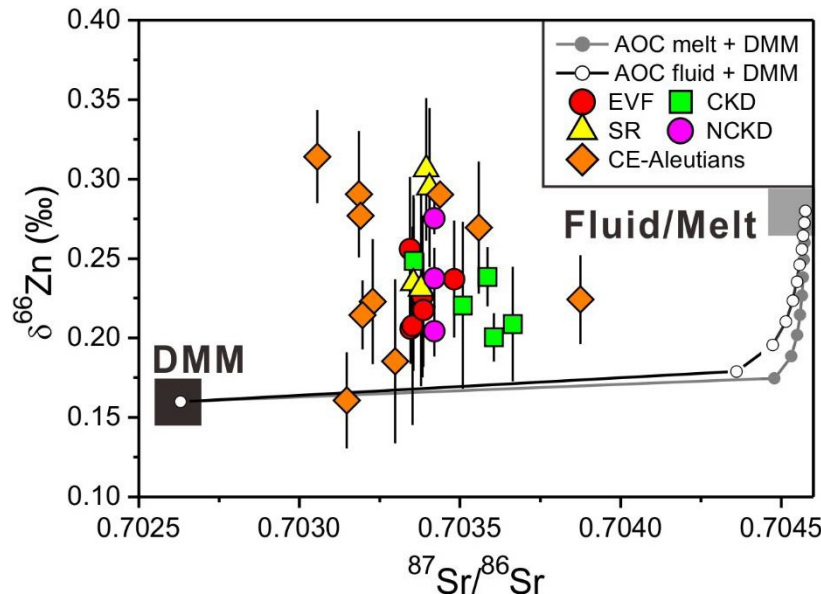


Fig. 8. $\delta^{66}\text{Zn}$ versus $^{87}\text{Sr}/^{86}\text{Sr}$ in the Kamchatka-Aleutian arc rocks in comparison to the mixing results between DMM and fluids/melts derived from subducted AOC. Modelling parameters for the average DMM are Zn = 55 ppm, Sr = 7.66 ppm, $\delta^{66}\text{Zn} = 0.16\text{\textperthousand}$, and $^{87}\text{Sr}/^{86}\text{Sr} = 0.702630$ (Salter and Stracke, 2004; Workman and Hart, 2005; Sossi et al., 2018). Isotopic compositions of AOC fluids and melts are assumed to equal to those of the AOC and adakitic melts studied here ($^{87}\text{Sr}/^{86}\text{Sr} = 0.704575$, $\delta^{66}\text{Zn} = 0.28$; Hochstaedter et al., 2001; this study). The elemental concentrations of AOC fluids are inferred from a high pressure vein within an eclogite with affinity of oceanic crust in South Western Tianshan (Li et al., 2013) and the modelled AOC fluids (Hochstaedter et al., 2001), which are Zn = 92.8 ppm and Sr = 558 ppm. AOC melts Sr (1316 ppm) and Zn (68.7 ppm) concentrations are represented by those of the adakites studied here (Abratis and Wörner, 2001; Wegner et al., 2011). Solid and open circles on lines denote 10% increments.

Experimental results of Extended X-Ray Absorption Fine Structure Spectroscopy (EXAFS) indicate that Zn has a tetrahedral coordination (^{IV}Zn) in basaltic melts with ^{IV}Zn-O distances of 1.95 Å (Dumas and Petiau, 1986; Le Grand et al., 2000). Divalent Zn (Zn^{2+}) has an ionic radius (0.74 Å) similar to those of Fe^{2+} (0.78 Å) and Mg^{2+} (0.72 Å) (Shannon, 1976) and substitutes for them on the tetrahedral sites of spinel and the octahedral sites of olivine and pyroxene. Mass balance calculations revealed that olivine and pyroxene account for >80–95% of the total Zn budget in peridotites (O'Reilly et al., 1991; Re Loux et al., 2010). The similar $\delta^{66}\text{Zn}$ between bulk rock, olivine, and pyroxene, despite of variable spinel modal abundances (0.80–2.9% by mass, Wang et al., 2017 and references therein), further suggests that olivine and pyroxene predominantly control the Zn isotopic budget of peridotites. Thus, the difference in $\delta^{66}\text{Zn}$ between basaltic melts and peridotites may be attributed to isotope fractionation between tetrahedrally co-ordinated Zn (^{IV} Zn^{2+}) in the melts and octahedrally co-ordinated Zn (^{VI} Zn^{2+}) in residual mantle minerals (Sossi et al., 2018) because the former has a shorter Zn-O bond and thus prefers heavier isotopes relative to the latter (Schauble, 2004; Sossi and O'Neill, 2017).

Zinc isotopic measurements of mineral separates documented that the equilibrium fractionation factor of Zn isotopes between olivine and spinel is $-0.13\text{\textperthousand}$ at $\sim 850^\circ\text{C}$ (i.e., $\Delta^{66}\text{Zn}_{\text{Ol-Sp}} = \delta^{66}\text{Zn}_{\text{Ol}} - \delta^{66}\text{Zn}_{\text{Sp}} = -0.13\text{\textperthousand}$) (Wang et al., 2017). Taking the effect of temperature on isotope fractionation factors into account, Sossi et al. (2018) obtained $\Delta^{66}\text{Zn}_{\text{Ol-Sp}} = -0.17 \times 10^6/\text{T}^2$ (T in Kelvin). Accordingly,

$\Delta^{66}\text{Zn}_{\text{Cpx-Sp}} \approx \Delta^{66}\text{Zn}_{\text{Opx-Sp}} \approx \Delta^{66}\text{Zn}_{\text{Ol-Sp}} = -0.17 \times 10^6/\text{T}^2$ because clinopyroxene and orthopyroxene have Zn isotopic compositions similar to olivine (Wang et al., 2017). It is noted that peridotitic spinel and basaltic melts have an identical $\delta^{66}\text{Zn}$ of $\sim 0.28\text{\textperthousand}$ (Wang et al., 2017), reflecting the same coordination number (CN = 4) of Zn^{2+} in spinel and basaltic melts (Dumas and Petiau, 1986; Le Grand et al., 2000). Thus, it is reasonable to assume that the Zn isotope fractionation factor between melts and spinel should be close to zero (i.e., $\Delta^{66}\text{Zn}_{\text{Melt-Sp}} = 0 \times 10^6/\text{T}^2$) during mantle partial melting (Sossi et al., 2018).

Although the mantle wedge is more depleted in incompatible elements than the mid-ocean ridge mantle (e.g., Woodhead et al., 1993; Nebel et al., 2015), the $\delta^{66}\text{Zn}$ of the Kamchatka-Aleutian arc rocks are similar to those of MORBs (Fig. 5a, c). This indicates that the effect of melt extraction on the Zn isotopic composition of the mantle is negligible, consistent with the results of komatiites and mantle peridotites (Sossi et al., 2018). We therefore suggest that the $\delta^{66}\text{Zn}$ of the mantle wedge is similar to that of the DMM and PM ($0.16 \pm 0.06\text{\textperthousand}$, Sossi et al., 2018). Based on the fractionation factors outlined above, we modeled the behavior of Zn isotopes during mantle melting using the non-modal and fractional melting equations developed for isotope partitioning by Sossi and O'Neill (2017). The parameters for modeling and the modeled Zn isotopic compositions of primary melts are outlined in Fig. 9 where we compared the modeled results with the $\delta^{66}\text{Zn}$ of the Kamchatka and CE-Aleutian arc rocks. According to fractionation-corrected major and trace element

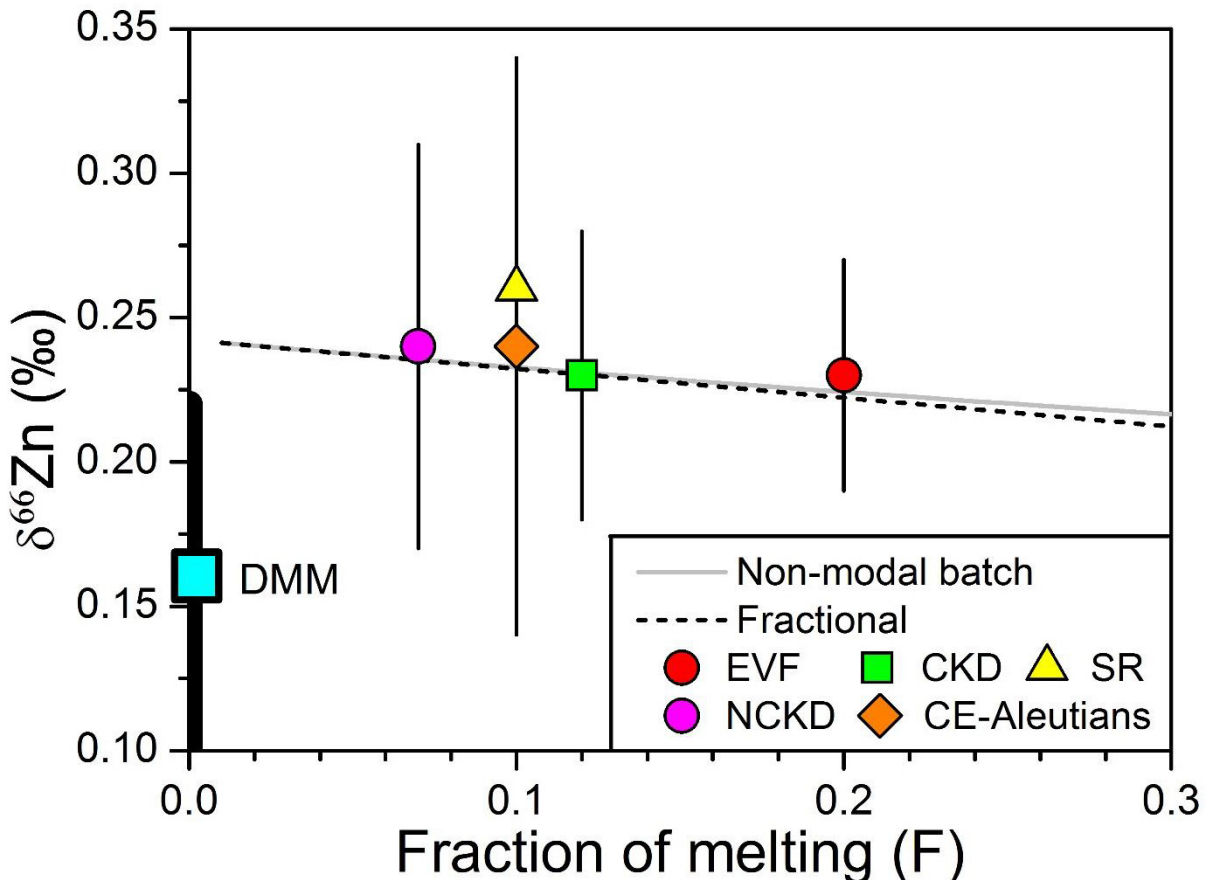


Fig. 9. Average $\delta^{66}\text{Zn}$ of arc rocks in individual locations in comparison to those of primary magmas generated using two melting models. Non-modal batch and fractional melting models are adopted from Sossi et al. (2018) and Sossi and O'Neill (2017). The DMM source has a mineral modal abundance of 57% for olivine, 28% for orthopyroxene, 13% for clinopyroxene, and 2% for spinel (Workman and Hart, 2005) and $\delta^{66}\text{Zn}$ of 0.16‰ (Sossi et al., 2018). The melting reaction is $0.652\text{Opx} + 0.470\text{Cpx} + 0.049\text{Sp} = 1\text{Melt} + 0.167\text{Ol}$ (Niu, 1997). Partition coefficients ($_{\text{mineral-melt}}D_{\text{Zn}}$) are 0.96 for olivine, 0.45 for orthopyroxene, 0.33 for clinopyroxene, and 5.2 for spinel (Davis et al., 2013). Fractionation factors between melt and mineral ($\Delta^{66}\text{Zn}_{\text{melt-mineral}}$) are $0.17 \times 10^6/\text{T}^2$ for olivine, orthopyroxene, and clinopyroxene and $0 \times 10^6/\text{T}^2$ for spinel (Sossi et al., 2018). Temperature for the melting zone of the sub-arc mantle is assumed to be 1473 K (Manning, 2004).

concentrations at $\text{MgO} = 6$ wt%, Churikova et al. (2001) proposed that degrees of mantle melting are $\sim 7\%$ for NCKD, $\sim 12\%$ for CKD, $\sim 10\%$ for SR, and 20% for EVF rocks. Cai et al. (2015) suggested that the CE-Aleutian magmas were formed by $\sim 10\%$ partial melting. Because of limited Zn isotope fractionation during differentiation of arc magmas outlined in Section 5.1, we use the average $\delta^{66}\text{Zn}$ of rocks in individual locations to represent those of primary melts for comparison. In the plot of $\delta^{66}\text{Zn}$ versus melting fraction (F in Fig. 9), the $\delta^{66}\text{Zn}$ values in modeled primary melts overlap with those in the Kamchatka-Aleutian arc rocks. This implies that their Zn isotopic compositions could be predominantly controlled by partial melting of the mantle wedge.

6. CONCLUSIONS

High precision Zn isotopic analyses were performed for 37 well-characterized subduction-related rocks from the Kamchatka and CE Aleutian arcs. Combining with Zn isotopic data for seven MORBs, two BABBs and nine adakites, the following conclusions can be made:

- (1) Magmas at convergent plate margins have $\delta^{66}\text{Zn}$ from 0.16 to 0.31‰, similar to those erupted in mid-oceanic ridges, back-arc basins, and ocean islands.
- (2) The $\delta^{66}\text{Zn}$ values are not clearly correlated with indicators of magma differentiation (e.g., MgO , SiO_2 , and Zn/Fe_T) or subduction components (e.g., Ba/La , Ba/Th , Sr/Y , Hf/Lu , and $^{87}\text{Sr}/^{86}\text{Sr}$), suggesting that magma differentiation and slab-derived fluids/melts have a limited influence on the Zn isotopic budget of arc magmas.
- (3) Most arc magmas have statistically higher $\delta^{66}\text{Zn}$ ($>0.22\text{\textperthousand}$) than that of the DMM ($0.16 \pm 0.06\text{\textperthousand}$, Sossi et al., 2018). This discrepancy can be explained by Zn isotope fractionation during partial melting of the mantle wedge with melts being enriched in heavier isotopes relative to the residual mantle.

ACKNOWLEDGEMENTS

This study is financially supported by grants from the National Key R&D Program of China (No. 2016YFC0600404) and the

National Natural Science Foundation of China (Nos. 41773002, 41573018, 41630206). We gratefully thank Y. Cai, S. Huang, C. Langmuir, and H. Sigurdsson for providing precious samples. We gratefully acknowledge Dr. Paolo Sossi and two anonymous reviewers for thorough and constructive reviews, and Dr. James Day for comments and the editorial handling, which greatly improve this manuscript.

REFERENCES

- Abratis M. and Wörner G. (2001) Ridge collision, slab-window formation, and the flux of Pacific asthenosphere into the Caribbean realm. *Geology* **29**, 127–130.
- Arevalo, Jr. R. and McDonough W. F. (2010) Chemical variations and regional diversity observed in MORB. *Chem. Geol.* **271**, 70–85.
- Bézos Antoin, Escrig Stéphan, Langmuir Charles H., Michael Peter J. and Asimow Paul D. (2009) Origins of chemical diversity of back-arc basin basalts: a segment-scale study of the Eastern Lau Spreading Center. *J. Geophys. Res.* **114**, 1–25.
- Bentahila Y., Ben Othman D. and Luck J.-M. (2008) Strontium, lead and zinc isotopes in marine cores as tracers of sedimentary provenance: a case study around Taiwan orogen. *Chem. Geol.* **248**, 62–82.
- Cai Y., LaGatta A., Goldstein S. L., Langmuir C. H., Gómez-Tuena A., Martín-del Pozzo A. L. and Carrasco-Núñez G. (2014) Hafnium isotope evidence for slab melt contributions in the Central Mexican Volcanic Belt and implications for slab melting in hot and cold slab arcs. *Chem. Geol.* **377**, 45–55.
- Cai Y., Rioux M., Kelemen P. B., Goldstein S. L., Bolge L. and Kylander-Clark A. R. C. (2015) Distinctly different parental magmas for calc-alkaline plutons and tholeiitic lavas in the central and eastern Aleutian arc. *Earth Planet. Sci. Lett.* **431**, 119–126.
- Chen H., Savage P. S., Teng F.-Z., Helz R. T. and Moynier F. (2013) Zinc isotope fractionation during magmatic differentiation and the isotopic composition of the bulk Earth. *Earth. Planet. Sci. Lett.* **369–370**, 34–42.
- Chen J.-B., Gaillardet J., Dessert C., Villemant B., Louvat P., Crispi O., Birck J.-L. and Wang Y.-N. (2014) Zn isotope compositions of the thermal spring waters of La Soufrière volcano, Guadeloupe Island. *Geochim. Cosmochim. Acta* **127**, 67–82.
- Chen S., Liu Y., Hu J., Zhang Z., Hou Z., Huang F. and Yu H. (2016) Zinc isotopic compositions of NIST SRM 683 and whole-rock reference materials. *Geostand. Geoanalyt. Res.* **40**, 417–432.
- Churikova T., Dorendorf F. and Wörner G. (2001) Sources and fluids in the mantle wedge below Kamchatka, evidence from across-arc geochemical variation. *J. Petrol.* **42**, 1567–1593.
- Churikova T., Wörner G., Mironov N. and Kronz A. (2007) Volatile (S, Cl and F) and fluid mobile trace element compositions in melt inclusions: implications for variable fluid sources across the Kamchatka arc. *Contrib. Mineral. Petrol.* **154**, 217–239.
- Defant M. J. and Drummond M. S. (1990) Derivation of some modern arc magmas by melting of young subducted lithosphere. *Nature* **347**, 662–665.
- Dorendorf F., Wiechert U. and Wörner G. (2000) Hydrated sub-arc mantle: a source for the Kluchevskoy volcano, Kamchatka/Russia. *Earth Planet. Sci. Lett.* **175**, 69–86.
- Doucet L. S., Mattielli N., Ionov D. A., Debouge W. and Golovin A. V. (2016) Zn isotopic heterogeneity in the mantle: a melting control? *Earth Planet. Sci. Lett.* **451**, 232–240.
- Du D.-H., Wang X.-L., Yang T., Chen X., Li J.-Y. and Li W. (2017) Origin of heavy Fe isotope compositions in high-silica igneous rocks: a rhyolite perspective. *Geochim. Cosmochim. Acta* **218**, 58–72.
- Dumas T. and Petiau J. (1986) EXAFS study of titanium and zinc environments during nucleation in a cordierite glass. *J. Non-Crystall. Solids* **81**, 201–220.
- Drummond M. S. and Defant M. J. (1990) A Model for trondhjemite-tonalite-dacite genesis and crystal growth via slab melting: Archean to modern comparisons. *J. Geophys. Res.* **95**, 21503–21521.
- Elliott T., Plank T., Zindler A., White W. and Bourdon B. (1997) Element transport from slab to volcanic front at the Mariana arc. *J. Geophys. Res.* **102**, 14991–15019.
- Ewart A. and Griffin W. L. (1994) Application of proton-microprobe data to trace-element partitioning in volcanic rocks. *Chem. Geol.* **117**, 251–284.
- Gale A., Dalton C. A., Langmuir C. H., Su Y. and Schilling J.-G. (2013) The mean composition of ocean ridge basalts. *Geochem., Geophys., Geosyst.* **14**, 489–518.
- Geist E. L. and Scholl D. W. (1994) Large-scale deformation related to the collision of the Aleutian Arc with Kamchatka. *Tectonics* **13**, 538–560.
- Hawkesworth C., Turner S., Peate D., McDermott F. and Calstern P. V. (1997) Elemental U and Th variations in island arc rocks: implications for U-series isotopes. *Chem. Geol.* **139**, 207–221.
- Helz R. T. (1987) Differentiation behaviour of Kilauea Iki lava lake, Kilauea Volcano, Hawaii: an overview of past and current work. In *Magmatic Processes: Physiochemical Principles* (ed. B. O. Mysen). Geochemical Society, St.Louis, pp. 241–258.
- Helz R. T. (2009) Processes active in mafic magma chambers: the example of Kilauea Iki Lava Lake, Hawaii. *Lithos* **111**, 37–46.
- Herrstrom E. A., Reagan M. K. and Morris J. D. (1995) Variations in lava composition associated with flow of asthenosphere beneath southern Central America. *Geology* **23**, 617–620.
- Herzog G. F., Moynier F., Albarède F. and Bereznov A. A. (2009) Isotopic and elemental abundances of copper and zinc in lunar samples, Zagami, Pele's hairs, and a terrestrial basalt. *Geochim. Cosmochim. Acta* **73**, 5884–5904.
- Hochstaedter A., Gill J., Peters R., Broughton P., Holden P. and Taylor B. (2001) Across-arc geochemical trends in the Izu-Bonin arc: contributions from the subducting slab. *Geochem. Geophys. Geosyst.* **2**, 1019.
- Huang J., Liu S.-A., Wörner G., Yu H. and Xiao Y. (2016) Copper isotope behavior during extreme magma differentiation and degassing: a case study on Laacher See phonolite tephra (East Eifel, Germany). *Contrib. Miner. Petrol.* **171**, 1–16.
- Huang S. and Frey F. A. (2003) Trace element abundances of Mauna Kea basalt from phase 2 of the Hawaii Scientific Drilling Project: petrogenetic implications of correlations with major element content and isotopic ratios. *Geochem., Geophys., Geosyst.* **4**, 8711.
- Inglis E. C., Debret B., Burton K. W., Millet M.-A., Pons M.-L., Dale C. W., Bouilhol P., Cooper M., Nowell G. M., McCoy-West A. J. and Williams H. M. (2017) The behavior of iron and zinc stable isotopes accompanying the subduction of mafic oceanic crust: a case study from Western Alpine ophiolites. *Geochem. Geophys. Geosyst.* **18**, 2562–2579.
- Jenner F. E. and O'Neill H. S. C. (2012) Major and trace analysis of basaltic glasses by laser-ablation ICP-MS. *Geochem. Geophys. Geosyst.* **13**, Q03003.
- Kay R. W. (1978) Aleutian magnesian andesites:melts from subducted Pacific ocean crust. *J. Volcan. Geoth. Res.* **4**, 117–132.

- Kelemen P. B., Høghøj K. and Greene A. R. (2007) 3.18 – One view of the geochemistry of subduction-related Magmatic Arcs, with an Emphasis on Primitive Andesite and Lower Crust A2 - Holland, Heinrich D. In *Treatise on Geochemistry* (ed. K. K. Turekian). Pergamon, Oxford, pp. 1–70.
- König S., Wille M., Voegelin A. and Schoenberg R. (2016) Molybdenum isotope systematics in subduction zones. *Earth Planet. Sci. Lett.* **447**, 95–102.
- Kogiso T., Tatsumi Y. and Nakano S. (1997) Trace element transport during dehydration processes in the subducted oceanic crust: 1. Experiments and implications for the origin of ocean island basalts. *Earth Planet. Sci. Lett.* **148**, 193–205.
- Lee C.-T. A., Luffi P., Le Roux V., Dasgupta R., Albarède F. and Leeman W. P. (2010) The redox state of arc mantle using Zn/Fe systematics. *Nature* **468**, 681–685.
- Le Grand M., Ramos A. Y., Calas G., Galois L., Ghaleb D. and Pacaud F. (2000) Zinc environment in aluminoborosilicate glasses by Zn K-edge extended X-ray absorption fine structure spectroscopy. *J. Mater. Res.* **15**, 2015–2019.
- Le Roux V., Lee C. T. A. and Turner S. J. (2010) Zn/Fe systematics in mafic and ultramafic systems: implications for detecting major element heterogeneities in the Earth's mantle. *Geochim. Cosmochim. Acta* **74**, 2779–2796.
- Li J.-L., Gao J., John T., Klemd R. and Su W. (2013) Fluid-mediated metal transport in subduction zones and its link to arc-related giant ore deposits: constraints from a sulfide-bearing HP vein in lawsonite eclogite (Tianshan, China). *Geochim. Cosmochim. Acta* **120**, 326–362.
- Little S. H., Vance D., Walker-Brown C. and Landing W. M. (2014) The oceanic mass balance of copper and zinc isotopes, investigated by analysis of their inputs, and outputs to ferromanganese oxide sediments. *Geochim. Cosmochim. Acta* **125**, 673–693.
- Little S. H., Vance D., McManus J. and Severmann S. (2016) Key role of continental margin sediments in the oceanic mass balance of Zn and Zn isotopes. *Geology* **44**, 207–210.
- Liu S.-A., Huang J., Liu J., Wörner G., Yang W., Tang Y.-J., Chen Y., Tang L., Zheng J. and Li S. (2015) Copper isotopic composition of the silicate Earth. *Earth Planet. Sci. Lett.* **427**, 95–103.
- Liu S.-A., Wang Z.-Z., Li S.-G., Huang J. and Yang W. (2016) Zinc isotope evidence for a large-scale carbonated mantle beneath eastern China. *Earth Planet. Sci. Lett.* **444**, 169–178.
- Manning C. E. (2004) The chemistry of subduction-zone fluids. *Earth Planet. Sci. Lett.* **223**, 1–16.
- Maréchal C. N., Nicolas E., Douchat C. and Albarède F. (2000) Abundance of zinc isotopes as a marine biogeochemical tracer. *Geochim. Geophys. Geosyst.* **1**, 1015. <https://doi.org/10.1029/1999GC000029>.
- McCulloch M. T. and Gamble J. A. (1991) Geochemical and geodynamical constraints on subduction zone magmatism. *Earth Planet. Sci. Lett.* **102**, 358–374.
- Münker C., Wörner G., Yogodzinski G. and Churikova T. (2004) Behaviour of high field strength elements in subduction zones: constraints from Kamchatka-Aleutian arc lavas. *Earth Planet. Sci. Lett.* **224**, 275–293.
- Métrich N. and Wallace P. J. (2008) Volatile abundances in basaltic magmas and their degassing paths tracked by melt inclusions. *Re. Miner. Geochem.* **69**, 363–402.
- Maréchal C. N., Télouk P. and Albarède F. (1999) Precise analysis of copper and zinc isotopic compositions by plasma-source mass spectrometry. *Chem. Geol.* **156**, 251–273.
- Moeller K., Schoenberg R., Pedersen R.-B., Weiss D. and Dong S. (2012) Calibration of the new certified reference materials ERM-AE633 and ERM-AE647 for Copper and IRMM-3702 for Zinc Isotope Amount Ratio Determinations. *Geostand. Geoanal. Res.* **36**, 177–199.
- Nebel O., Sossi P. A., Bénard A., Wille M., Vroon P. Z. and Arculus R. J. (2015) Redox-variability and controls in subduction zones from an iron-isotope perspective. *Earth Planet. Sci. Lett.* **432**, 142–151.
- Niu Y. (1997) Mantle melting and melt extraction processes beneath ocean ridges: evidence from Abyssal Peridotites. *J. Petrol.* **38**, 1047–1074.
- O'Reilly S. Y., Griffin W. L. and Ryan C. G. (1991) Residence of trace elements in metasomatized spinel lherzolite xenoliths: a proton-microprobe study. *Contrib. Miner. Petrol.* **109**, 98–113.
- Pearce J. A. and Peate D. W. (1995) Tectonic implications of the composition of volcanic ARC magmas. *Annu. Rev. Earth Planet. Sci.* **23**, 251–285.
- Pichat S., Douchet C. and Albarède F. (2003) Zinc isotope variations in deep-sea carbonates from the eastern equatorial Pacific over the last 175 ka. *Earth Planet. Sci. Lett.* **210**, 167–178.
- Pons M.-L., Quitté G., Fujii T., Rosing M. T., Reynard B., Moynier F., Douchet C. and Albarède F. (2011) Early Archean serpentine mud volcanoes at Isua, Greenland, as a niche for early life. *Proc. Natl. Acad. Sci.* **108**, 17639–17643.
- Pons M.-L., Debret B., Bouilhol P., Delacour A. and Williams H. (2016) Zinc isotope evidence for sulfate-rich fluid transfer across subduction zones. *Nat. Commun.* **7**, 13794.
- Salters V. J. M. and Stracke A. (2004) Composition of the depleted mantle. *Geochim. Geophys. Geosyst.* **5**, Q05B07.
- Schauble E. A. (2004) Applying stable isotope fractionation theory to new systems. *Rev. Miner. Geochem.* **55**, 65–111.
- Schüssler J. A., Schoenberg R. and Sigmarsson O. (2009) Iron and lithium isotope systematics of the Hekla volcano, Iceland — evidence for Fe isotope fractionation during magma differentiation. *Chem. Geol.* **258**, 78–91.
- Shannon R. (1976) Revised effective ionic radii and systematic studies of interatomic distances in halides and chalcogenides. *Acta Crystallogr. Sect. A* **32**, 751–767.
- Sossi P. A., Nebel O., O'Neill H. S. C. and Moynier F. (2018) Zinc isotope composition of the Earth and its behaviour during planetary accretion. *Chem. Geol.* **471**, 125–135.
- Sossi P. A., Halverson G. P., Nebel O. and Eggin S. M. (2015) Combined separation of Cu, Fe and Zn from rock matrices and improved analytical protocols for stable isotope determination. *Geostand. Geoanal. Res.* **39**, 129–149.
- Sossi P. A., Nebel O. and Foden J. (2016) Iron isotope systematics in planetary reservoirs. *Earth. Planet. Sci. Lett.* **452**, 295–308.
- Sossi P. A. and O'Neill H. S. C. (2017) The effect of bonding environment on iron isotope fractionation between minerals at high temperature. *Geochim. Cosmochim. Acta* **196**, 121–143.
- Tang M., Rudnick R. L. and Chauvel C. (2014) Sedimentary input to the source of Lesser Antilles lavas: a Li perspective. *Geochim. Cosmochim. Acta* **144**, 43–58.
- Teng F.-Z., Hu Y. and Chauvel C. (2016) Magnesium isotope geochemistry in arc volcanism. *Proc. Natl. Acad. Sci.* **113**, 7082–7087.
- Teng F. Z., Dauphas N. and Helz R. T. (2008) Iron isotope fractionation during magmatic differentiation in Kilauea Iki Lava Lake. *Science* **320**, 1620–1622.
- Tibaldi A. and Bonali F. L. (2017) Intra-arc and back-arc volcanotectonics: Magma pathways at Holocene Alaska-Aleutian volcanoes. *Earth Sci. Rev.* **167**, 1–26.
- Toutain J.-P., Sonke J., Munoz M., Nonell A., Polvé M., Viers J., Freydier R., Sortino F., Joron J.-L. and Sumarti S. (2008) Evidence for Zn isotopic fractionation at Merapi volcano. *Chem. Geol.* **253**, 74–82.

- Wang Z.-Z., Liu S.-A., Liu J., Huang J., Xiao Y., Chu Z.-Y., Zhao X.-M. and Tang L. (2017) Zinc isotope fractionation during mantle melting and constraints on the Zn isotope composition of Earth's upper mantle. *Geochim. Cosmochim. Acta* **198**, 151–167.
- Wegner W., Wörner G., Harmon R. S. and Jicha B. R. (2011) Magmatic history and evolution of the Central American Land Bridge in Panama since Cretaceous times. *Geol. Soc. Amer. Bull.* **123**, 703–724.
- Woodhead J., Eggins S. and Gamble J. (1993) High field strength and transition element systematics in island arc and back-arc basin basalts: evidence for multi-phase melt extraction and a depleted mantle wedge. *Earth Planet. Sci. Lett.* **114**, 491–504.
- Workman R. K. and Hart S. R. (2005) Major and trace element composition of the depleted MORB mantle (DMM). *Earth Planet. Sci. Lett.* **231**, 53–72.
- Yogodzinski G. M., Kay R. W., Volynets O. N., Koloskov A. V. and Kay S. M. (1995) Magnesian andesite in the western Aleutian Komandorsky region: implications for slab melting and processes in the mantle wedge. *Geol. Soc. Amer. Bull.* **107**, 505–519.
- Yogodzinski G. M., Lees J. M., Churikova T. G., Dorendorf F., Woerner G. and Volynets O. N. (2001) Geochemical evidence for the melting of subducting oceanic lithosphere at plate edges. *Nature* **409**, 500–504.
- Yogodzinski G. M., Brown S. T., Kelemen P. B., Vervoort J. D., Portnyagin M., Sims K. W. W., Hoernle K., Jicha B. R. and Werner R. (2015) The role of subducted Basalt in the Source of Island Arc Magmas: evidence from seafloor Lavas of the Western Aleutians. *J. Petrol.* **56**, 441–492.

Associate Editor: James M.D. Day